

1 A Multi-resolution Gaussian process model for the analysis  
2 of large spatial data sets.

3 Douglas Nychka, Soutir Bandyopadhyay, Dorit Hammerling,  
4 Finn Lindgren, and Stephan Sain \*

4 August 13, 2013

5 **Abstract**

6 A multi-resolution model is developed to predict two-dimensional spatial fields based  
7 on irregularly spaced observations. The radial basis functions at each level of resolution  
8 are constructed using a Wendland compactly supported correlation function with the nodes  
9 arranged on a rectangular grid. The grid at each finer level increases by a factor of two  
10 and the basis functions are scaled to have a constant overlap. The coefficients associated  
11 with the basis functions at each level of resolution are distributed according to a Gaussian  
12 Markov random field (GMRF) and take advantage of the fact that the basis is organized  
13 as a lattice. Several numerical examples and analytical results establish that this scheme  
14 gives a good approximation to standard covariance functions such as the Matérn and also  
15 has flexibility to fit more complicated shapes. The other important feature of this model is  
16 that it can be applied to statistical inference for large spatial datasets because key matrices  
17 in the computations are sparse. The computational efficiency applies to both the evaluation  
18 of the likelihood and spatial predictions.

19 *Keywords:* Spatial estimator, Kriging, Fixed Rank Kriging, Sparse Cholesky Decomposi-  
20 tion, Multi-resolution

21 **1 Introduction**

22 Statistical methodology for spatial data is a well developed field and has roots in  
23 geostatistics and multivariate analysis. More recently the breakthroughs in Bayesian  
24 hierarchical models have added rich new classes of models for handling heterogenous

---

\*Douglas Nychka, is Senior Scientist, National Center for Atmospheric Research, PO Box 3000, Boulder CO 30307-3000 (nychka@ucar.edu), Soutir Bandyopadhyay, is Assistant Professor, Lehigh University, Bethlehem, PA, 18015, Dorit Hammerling is Post Doctoral Scientist, Statistical and Applied Mathematical Sciences Institute, Research Triangle Park, NC, 27709-4006, Finn Lindgren is Lecturer, University of Bath, Bath, BA2 7AY, UK and Stephan Sain is Scientist, National Center for Atmospheric Research, PO Box 3000, Boulder CO 30307-3000.

25 spatial data and indirect measurements of spatial processes (Banerjee et al. (2003),  
 26 Cressie and Wikle (2011)). This development in spatial statistics is coincident with  
 27 emerging challenges in the geosciences involving new types of observations and com-  
 28 parisons of such observations to complex numerical models. For example, as attention  
 29 in climate science shifts to understanding the regional and local changes in future cli-  
 30 mate there is a need to analyze high resolution simulations from climate models and  
 31 to compare them to surface and remotely sensed observations at fine levels of details.  
 32 These kinds of geoscience applications are characterized by large numbers of spatial  
 33 locations. The application of standard techniques is often not feasible or at least will  
 34 take an unacceptably long time given standard algorithms and typical computational  
 35 resources. Moreover, geophysical processes tend to have a multi-scale character over  
 36 space that requires statistical methods that allow for potentially complicated spatial  
 37 dependence beyond a simple parametric model that adjusts for a correlation range  
 38 and process smoothness. This work develops a new statistical model that addresses  
 39 both of these challenges; our model is applicable to large data sets and supports a  
 40 more flexible covariance structure that can be a mixture of more standard covariance  
 41 functions. Thus our model fills a gap in current statistical methodology.

42 We assume that spatial observations  $\{\mathbf{y}_i\}$  are made at unique two-dimensional  
 43 spatial locations,  $\{\mathbf{x}_i\}$ , for  $1 \leq i \leq n$ , according to the additive model:

$$\mathbf{y}_i = Z_i^T \mathbf{d} + g(\mathbf{x}_i) + \epsilon_i, \quad (1)$$

44 where  $Z$  is a matrix of covariates and  $\mathbf{d}$  a vector of linear parameters,  $g$  is a smooth  
 45 Gaussian process and  $\epsilon_i$  are mean zero measurement errors. The parameters  $\mathbf{d}$  repre-  
 46 sent fixed effects in this model.

47 The statistical problem in this setting is to determine  $g$  at locations where observa-  
 48 tions are not available and quantify the uncertainty of the spatial predictions. Given  
 49 our main goal to develop an acceptable methodology to handle large data sets, we seek  
 50 to balance the complexity of the models and methodology with feasibility for effective  
 51 data analysis. We will focus on maximum likelihood estimates of parameters in the  
 52 covariance and other model components. For prediction we will adopt the conditional  
 53 distribution of  $g$  given the data and other statistical parameters. Our approach com-

54 bins the representation of a field using a multi-resolution (MR) basis with statistical  
 55 models for the coefficients as a process on a lattice. In this sense it is a blending of  
 56 ideas from fixed rank Kriging (Katzfuss and Cressie 2011, Cressie and Johannesson  
 57 2008) and stochastic partial differential equations (SPDE) including the work in Lind-  
 58 gren and Rue (2007), Rue and Held (2005) and Lindgren et al. (2011) (LR2011). It is  
 59 useful to view the unknown spatial process in (1) as a sum of  $L$  independent processes,  
 60  $g_l(\mathbf{x})$ , for  $1 \leq l \leq L$ , marginal variances  $\{\rho\alpha_l\}$ , and

$$g(\mathbf{x}) = \sum_{l=1}^L g_l(\mathbf{x}), \quad (2)$$

61 Here the parameter  $\rho > 0$  is useful as a leading scaling parameter for the covariance  
 62 matrix and the elements of  $\boldsymbol{\alpha}$  sum to one. In this way the overall spatial dependence  
 63 of  $g$  can be much more complex than the spatial dependence of each of the individual  
 64 components. Each component,  $g_l$  is defined through a basis function expansion as

$$g_l(\mathbf{x}) = \sum_{j=1}^{m(l)} c_j^l \phi_{j,l}(\mathbf{x}). \quad (3)$$

65 where  $\phi_j^l$ ,  $1 \leq j \leq m(l)$ , is a sequence of fixed basis functions and  $\mathbf{c}^l$  is a vector  
 66 of coefficients distributed multivariate normal with mean zero and covariance matrix,  
 67  $\rho\mathbf{P}_l$ .  $\mathbf{P}_l$  may also depend on additional parameters. Thus the model for  $g$  is a sum of  
 68 fixed basis functions with stochastic coefficients.

69 Our two main ideas address the basis functions and the covariance model for the  
 70 coefficients. We use families of radial basis functions that are organized on regular grids  
 71 of increasing resolution. These radial basis functions have compact support and like  
 72 wavelet bases give computational efficiencies because of this feature. In our treatment,  
 73 each increase in resolution will be by a factor of two and the levels associated with  
 74 finer spatial scales will have more basis functions. Conversely, the representation has a  
 75 parsimony in that the coarser scales require fewer basis functions to approximate the  
 76 stochastic processes. The spatial dependence among the coefficients for each level of  
 77 resolution is modeled using a Gaussian Markov random field (GMRF), specifically a  
 78 spatial autoregressive (SAR) model. The fact that the basis functions are organized  
 79 on a lattice gives the SAR a simple form along with its precision matrix, which we

80 denote as  $\mathbf{Q}_l = \mathbf{P}_l^{-1}$ . The benefit of this approach is that  $\mathbf{Q}_l$  is sparse even though  
81  $\mathbf{P}_l$  itself can be dense. Thus,  $g_l$  can exhibit long range correlations among coefficients  
82 widely separated in the lattice even though the precision matrix is sparse.

83 We have found that this combination of MR bases with companion GMRFs for the  
84 coefficients at each level can approximate standard families of covariance functions such  
85 as the Matérn, but also provides a rich model for more general spatial dependence. It  
86 should be noted that we make no assumption on the observation or prediction locations  
87 even though the latent components of our model will exploit regular grids. We are also  
88 able to give some analytical results that suggest why this model can approximate a  
89 range of spatial processes exhibiting different degrees of smoothness.

90 Many of the ingredients for this model are not new, however, their particular com-  
91 bination with a view towards efficient computations for large and irregular spatial data  
92 sets has not been exploited in previous works. The key is to introduce sparsity into the  
93 computations in a way that does not compromise covariance models with long range  
94 correlations and models with many degrees of freedom. This is achieved by using com-  
95 pactly supported radial basis functions and computing directly the *precision* matrix of  
96 the basis coefficients, not the covariance matrix. In addition we add a normalization of  
97 the marginal process variance that can reduce the degree of artifacts from using a dis-  
98 crete basis. The net result is a flexible covariance model that has rank comparable or  
99 greater than the number of spatial locations and where spatial prediction, conditional  
100 simulation and evaluation of the likelihood can be done on a modest laptop computer.

101 Recent work on statistical methods for large spatial data sets has used a fixed  
102 rank Kriging approach to make computations feasible. This can either take the form  
103 of a small number of basis functions and an unstructured and dense  $\mathbf{P}$  matrix such  
104 as in Cressie and Johannesson (2008) or large number of basis and a sparse model  
105 such a Markov random field for  $\mathbf{Q}$  (Eidsvik et al. 2010). An insightful approach  
106 was suggested in Stein (2008) and later in Sang and Huang (2011) where a low rank  
107 process was combined with a process that has a compactly supported covariance. This  
108 superposition of two processes anticipates our model where we consider a mixture  
109 of covariances at multiple scales. Reflecting the fact that the likelihood calculation

110 carries most of the computational cost, there has been work on approximations to the  
 111 likelihood for spatial models by binning the observations and using spectral methods  
 112 (Fuentes 2007) or considering a partial likelihood (Michael L. Stein 2004) or pseudo  
 113 likelihood (Caragea and Smith 2007). Our approach differs from these papers in that  
 114 we are able to compute the likelihood exactly.

115 The next section describes the fixed rank Kriging model and its likelihood under  
 116 a setting where the process and measurement errors have a Gaussian distribution.  
 117 Section 3 outlines the computational algorithm and gives some timing results. The  
 118 approximation properties of this basis/lattice model are reported in Section 4 with  
 119 the proofs of the asymptotic results relegated to the Appendix. Section 5 provides an  
 120 example for a climate precipitation data set and Section 6 is our conclusions. Much of  
 121 the computations in this paper can be reproduced using the `LatticeKrig` package in  
 122 R, which serves as a supplement for implementing the numerical methods and a ready  
 123 source for the data set from Section 5.

## 124 2 The spatial model

### 125 2.1 Process and observational models

126 Although we have introduced  $g$  as a MR, to streamline notation in this section it is  
 127 convenient to view this model as  $g(\mathbf{x}) = \sum_{j=1}^m c_j \phi_j(\mathbf{x})$ , where we have combined the  
 128 MR bases into a single basis, the MR coefficients into a single coefficient vector, and  
 129  $m$  is the total number of basis functions.

130 Based on the set up in the introduction  $g$  will be a mean zero Gaussian process  
 131 with a covariance matrix  $\rho \mathbf{P}$  and covariance function:

$$COV(g(\mathbf{x}), g(\mathbf{x}')) = \sum_{j,k=1}^m \rho \mathbf{P}_{j,k} \phi_j(\mathbf{x}), \phi_k(\mathbf{x}'). \quad (4)$$

132 with  $\mathbf{P}$  having dimension  $m \times m$ .

133 With respect to the observation model in (1) we assume that  $\epsilon_i$  are uncorrelated,  
 134 normally distributed with mean zero and covariance  $\sigma^2 \mathbf{W}^{-1}$ . Here we assume that  
 135  $\sigma^2$  is a free parameter of the measurement error distribution and  $\mathbf{W}$  is a known but

136 sparse precision matrix. In most applications  $\mathbf{W}$  is diagonal and we take  $\mathbf{W}$  to be the  
 137 identity for our example in Section 5. Let  $\Phi$  be the regression matrix with columns  
 138 indexing the basis functions and rows indexing locations.  $\Phi_{i,j} = \phi_j(\mathbf{x}_i)$ . With these  
 139 definitions one can now rewrite (1) in matrix vector notation as  $\mathbf{y} = \mathbf{Z}\mathbf{d} + \Phi\mathbf{c} + \mathbf{e}$  and  
 140 collecting the fixed and random components we have

$$\mathbf{y} \sim MN(\mathbf{Z}\mathbf{d}, \rho\Phi\mathbf{P}\Phi^T + \sigma^2\mathbf{W}^{-1}). \quad (5)$$

141 As a last step it is useful to reparametrize this model to better mesh with the  
 142 computations and in some instances to simplify formulas. Let  $\lambda = \sigma^2/\rho$  and we  
 143 reparametrize  $\sigma$  in terms of  $\lambda$  and  $\rho$  ( i.e.  $\sigma^2 = \lambda\rho$ ). Now set  $\mathbf{M}_\lambda = (\Phi\mathbf{P}\Phi^T + \lambda\mathbf{W}^{-1})$   
 144 and (5) is the same as  $\mathbf{y} \sim MN(\mathbf{Z}\mathbf{d}, \rho\mathbf{M}_\lambda)$ .

## 145 2.2 Spatial estimate

146 From (5) we have the log likelihood

$$\ell(\mathbf{y}|\rho, \mathbf{P}, \lambda, \mathbf{d}) = (-1/2)(\mathbf{y} - \mathbf{Z}\mathbf{d})^T(\rho\mathbf{M}_\lambda)^{-1}(\mathbf{y} - \mathbf{Z}\mathbf{d}) - (1/2)\log|\rho\mathbf{M}_\lambda| + (n/2)\log(\pi)$$

147 This expression is used to find maximum likelihood estimates (MLEs) of the fixed  
 148 effects and covariance parameters. For computation it is often convenient to first  
 149 maximize over the fixed effects and the covariance parameter  $\rho$  analytically to reduce  
 150 the number of parameters for optimization. For fixed  $\rho$  and  $\mathbf{P}$  the MLEs for  $\mathbf{d}$  are also  
 151 the generalized least squares (GLS) estimates

$$\hat{\mathbf{d}} = (\mathbf{Z}^T\mathbf{M}_\lambda^{-1}\mathbf{Z})^{-1}\mathbf{Z}^T\mathbf{M}_\lambda^{-1}\mathbf{y}. \quad (6)$$

152 Note this estimate only depends on  $\lambda$  and not on  $\rho$ . Set  $\mathbf{r} = \mathbf{y} - \mathbf{Z}\hat{\mathbf{d}}$  and substitute  
 153 back in the full log likelihood giving

$$\ell(\mathbf{y}|\rho, \mathbf{P}, \sigma, \hat{\mathbf{d}}) = (-1/2)(\mathbf{r}^T(\rho\mathbf{M}_\lambda)^{-1}\mathbf{r}) - (1/2)\log|\rho\mathbf{M}_\lambda| + (n/2)\log(\pi). \quad (7)$$

154 Finally, the expression given above can be maximized analytically over  $\rho$  giving  $\hat{\rho} =$   
 155  $\mathbf{r}^T\mathbf{M}_\lambda^{-1}\mathbf{r}/n$ . This estimate can be substituted back into (7) to give a *profile* log like-  
 156 lihood that only depends on  $\lambda = \sigma^2/\rho$  and on any other covariance parameters that  
 157 determine  $\mathbf{P}$ .

The inference for the basis coefficients depends on the standard results for the conditional normal distribution. Specifically, the conditional distribution of  $\mathbf{c}$  given  $\mathbf{y}$  and all other parameters in the model at their true values is a multivariate normal

$$[\mathbf{c}|\mathbf{y}, \mathbf{d}, \sigma, \rho, \mathbf{P}] \sim MN(\hat{\mathbf{c}}, \rho\mathbf{P} - \rho\mathbf{P}\Phi^T(\mathbf{M}_\lambda)^{-1}\Phi\mathbf{P}) \quad (8)$$

with

$$\hat{\mathbf{c}} = \mathbf{P}\Phi^T\mathbf{M}_\lambda^{-1}(\mathbf{y} - \mathbf{Z}\mathbf{d}) \quad (9)$$

This conditional mean,  $\hat{\mathbf{c}}$ , is taken to be the point estimate (or prediction) of  $\mathbf{c}$  and by linearity, the spatial prediction for  $g(\mathbf{x})$  at an arbitrary location is  $\hat{g}(\mathbf{x}) = \sum_{j=1}^m \phi_j(\mathbf{x})\hat{\mathbf{c}}_j$ . Typically a vector of the spatial covariates,  $\mathbf{z}(\mathbf{x})$ , is also provided at this location. To reproduce the familiar universal Kriging estimator,  $\mathbf{d}$  is set at the GLS estimate given above and so the full spatial prediction is:  $\hat{y}(\mathbf{x}) = \mathbf{z}(\mathbf{x})^T\hat{\mathbf{d}} + \hat{g}(\mathbf{x})$ .

## 2.3 Radial Basis functions (RBF)

Our full model proposes a MR basis where each level of resolution takes the same form and so we start with describing a single level of basis functions on a common scale. The basis functions are essentially translations and scalings of a single radial function. Let  $\phi$  be a unimodal, symmetric function in 1-dimension and let  $\{\mathbf{u}_j\}$ ,  $1 \leq j \leq m$  be a rectangular grid of points in two dimensions. Consistent with radial basis function terminology, we will refer to the grid points as *node points* and let  $\theta$  be a scale parameter. The basis functions are then

$$\phi_j^* = \phi(\|\mathbf{x} - \mathbf{u}_j\|/\theta) \quad (10)$$

Geometrically, the basis will consist of bumps centered at the node points with overlap controlled by the choice of  $\theta$ . In this work we will take  $\phi$  to be a two-dimensional Wendland covariance (Wendland 1995) that has support on  $[0, 1]$ . The Wendland functions are polynomials on  $[0, 1]$ . They are also positive definite, which is an attractive property when the basis is used for interpolation. In this work we use a Wendland function valid up to 3 dimensions and belonging to  $C^4$ :

$$\phi(d) = (1 - d)^6(35d^2 + 18d + 3)/3 \text{ for } 0 \leq d \leq 1, \text{ and zero otherwise.}$$

181 In all examples in this work we fix the scale factor to be 2.5 times the grid spacing.  
 182 Thus in two dimensions and away from edges each RBF overlaps with 68 others.

## 183 2.4 Markov Random fields

184 In parallel with the preceding section we describe the stochastic model for the coeffi-  
 185 cients of a basis constructed at a single level of resolution. The MR aspect replicates  
 186 this model at each level. The coefficient vector  $\mathbf{c}$  at a single level follows a Gaussian  
 187 Markov random field (GMRF) and is organized by the node points. We will assume the  
 188 special case that the coefficients follow a spatial autoregression (SAR). The difference  
 189 with this model for  $\mathbf{c}$  and that in LR2011 is that we define the SAR independently  
 190 from the choice of basis.

191 Given an autoregression matrix  $\mathbf{B}$  and  $\mathbf{e}$ , a random vector distributed as  $N(0, \rho I)$ ,  
 192 we construct the distribution of  $\mathbf{c}$  according to  $\mathbf{c} = \mathbf{B}^{-1}\mathbf{e}$ . The autoregressive interpre-  
 193 tation is that  $\mathbf{B}\mathbf{c} = \mathbf{e}$ . That is,  $\mathbf{B}$  transforms the correlated field to white noise with  
 194 variance  $\rho$ . For our use we will constrain  $\mathbf{B}$  to be sparse. Let  $\mathcal{N}_j$  denote the indices  
 195 of the nearest neighbors of  $\mathbf{u}_j$ . For an interior point this will be four neighbors, but  
 196 less for the nodes at edges and corners. Following LR2011 for interior lattice points we  
 197 take  $\mathbf{B}_{j,j} = 4 + \kappa^2$  with  $\kappa \geq 0$  and the off diagonal elements to be -1. Although one can  
 198 modify the weights at the edges of the lattice to approximate free boundary conditions,  
 199 we have found that adding a buffer and keeping zero boundary conditions provides an  
 200 easier solution. The boundary effects are also diminished by the normalization dis-  
 201 cussed in Section 2.6. By linearity  $\mathbf{c}$  has covariance matrix  $\rho\mathbf{B}^{-1}\mathbf{B}^{-T}$  and precision  
 202 matrix given by  $\mathbf{Q} = (1/\rho)\mathbf{B}^T\mathbf{B}$ . Because  $\mathbf{B}$  is formulated as unconditional weights  
 203 on the field, any choice of  $\mathbf{B}$  will lead to a valid covariance and so  $\mathbf{Q}$  will be positive  
 204 definite. It is well known that the SAR weights do not specify the Markov structure  
 205 directly. For nonzero weights on the four neighbors  $\mathbf{Q}$  will be a sparse matrix with each  
 206 row having 12 nonzero elements: the first, second and third order neighbors. Thus,  $\mathbf{c}$   
 207 will be a GMRF conditional on this larger clique of points. The results in LR2011 pro-  
 208 vide the connection between this GMRF and approximations to the Matérn family of  
 209 spatial covariances. In this particular case one expects that the SAR described above



will approximate a Matérn process with scale parameter  $\kappa$  in LR2011 and smoothness  $\nu = 1$ .

## 2.5 Extension to a MR process

In the previous sections we have developed a basis and a covariance for a specific grid. The MR model extends this idea by successively halving the spacing of the grid points and specifying a GMRF for the coefficients at each level. Between levels we assume coefficients are independent. To make this idea explicit assume that the spatial domain is the rectangle  $[a_1, a_2] \times [b_1, b_2]$  and the initial grid  $\{\mathbf{u}_j^1\}$  is laid out with  $m_x \times m_y$  grid points with the spacing  $\delta \equiv (a_2 - a_1)/(m_x - 1) = (b_2 - b_1)/(m_y - 1)$ . Note here the constraint that the spatial domain and numbers of grid points are matched so that the grid spacing is the same in the x and y dimensions. Subsequent grids are defined with spacings  $\delta_l = \delta 2^{-(l-1)}$  and yield a sequence of grids,  $\{\mathbf{u}_j^l\}$  that increase roughly by a factor of four in size from level  $l$  to level  $l + 1$ . To define the basis functions for the  $l^{\text{th}}$  level we take  $\theta_l = \theta/2^{(l-1)}$  and define the radial basis functions as in (10). Let  $L$  denote the total number of levels then the (unnormalized) MR basis is  $\phi_{j,l}^* = \phi(\|\mathbf{x} - \mathbf{u}_j^l\|/\theta_l)$ , where  $1 \leq l \leq L$ ,  $1 \leq j \leq m(l)$ , and  $m(l) = (m_x - 1)(m_y - 1)4^{l-1} + m_x + m_y + 1$ . The total number of basis functions is approximately  $(m_x m_y)(4^L)$ , (This is not exact because  $m$  grid points are subdivided into  $2m - 1$  points at the next level.) When buffer nodes are added to reduce edge effects we take these as a *fixed* number of extra points that are added to each edge of the grid. The number of basis functions follows a more complicated expression when buffer nodes are added at each level but is still grows at roughly  $4^L$ .

Recall that the vector of coefficients associated with each level is  $\mathbf{c}^l$  and the MR representation for  $g$  is given by equations (2) and (3) with either the unnormalized MR basis  $\{\phi_{j,l}^*\}$  or the normalized basis described in Section 2.6 below. It should be noted that the MR basis by itself does not contribute too much additional computation burden. The main difference in a single level of basis functions and a MR are additional nonzero elements in the inner matrix,  $\mathbf{\Phi}^T \mathbf{\Phi}$ , due to coarse resolution basis functions overlapping with finer resolution ones. Although the MR will have more nonzero

elements in the inner product matrix, there are many fewer coarse functions for overlap and so the total number of nonzero elements does not increase substantially. This feature can be seen in the timing results in Section 4.

It is useful to illustrate how the number of basis functions depend on the number of levels. Suppose that an initial grid of  $10 \times 10$  is chosen for a square spatial domain,  $L = 4$  and 5 extra, buffer node points are added on each side to moderate the edge effects. The first level, will comprise  $(10 + 10) \times (10 + 10) = 400$  grid points including a buffer region on all four sides of the spatial domain. The second level will decrease the grid spacing by a factor of two giving  $19 \times 19$  grid points included in the spatial domain and being aligned with the coarser grid. To these are appended 5 buffer points on each edge giving a total of  $29 \times 29 = 841$  points. Subsequent levels yield  $(37 + 10) \times (37 + 10) = 2209$  and  $(73 + 10) \times (73 + 10) = 6889$  grid points. The four levels sum to 10399 grid points/basis functions and of these 7159 have nodes that are included in the spatial domain.

In general we can stack these coefficients as  $\mathbf{c} = (\mathbf{c}^1, \mathbf{c}^2, \dots, \mathbf{c}^L)$  and the natural extension of the SAR model is a sparse matrix  $\mathbf{B}$  such that  $\mathbf{B}\mathbf{c}$  is  $N(0, \rho I)$ . Although  $\mathbf{B}$  can be a general matrix we have found it useful to restrict attention to a block diagonal form. Let  $\alpha_1, \alpha_2, \dots, \alpha_L$  be a vector of positive weights and for the  $l^{th}$  level we assume  $\mathbf{c}^l$  follow a GMRF with a SAR matrix,  $(1/\sqrt{\alpha_l})\mathbf{B}_l$ . Here  $\mathbf{B}_l$  has the same form as in the single level but with the  $\kappa$  parameter possibly depending on the level. One can interpret  $\rho\alpha_l$  as parameterizing the marginal variance of the  $l^{th}$  level process and  $\kappa_l$  is an approximate scale parameter. Thus we are lead to a block diagonal form for  $\mathbf{B}$  and also for the precision matrix:

$$\mathbf{Q} = (1/\rho) \begin{bmatrix} (1/\alpha_1)(\mathbf{B}_1)^T \mathbf{B}_1 & 0 & \dots & 0 \\ 0 & (1/\alpha_2)(\mathbf{B}_2)^T \mathbf{B}_2 & \dots & 0 \\ 0 & 0 & \dots & 0 \\ 0 & 0 & 0 & (1/\alpha_L)(\mathbf{B}_L)^T \mathbf{B}_L \end{bmatrix} \quad (11)$$

$\mathbf{Q}$  will have dimension  $m \times m$  equal to the total number of basis functions but of course will be sparse and  $\mathbf{c}$  will have length  $m$ .

## 2.6 Normalization to approximate stationarity

Based on the specific form for  $\mathbf{Q}$  we have found it useful to normalize the basis functions to give a better approximation to stationary covariance functions. It is well known that a GMRF on a finite lattice can exhibit edge effects and other artifacts in the covariance model that are not physical. Moreover the radial basis functions having nodes on a discrete set can also contribute to patterns in the implied covariance matrix. One obvious correction for this effect is to weight the basis functions so that when (4) is evaluated one will obtain a constant marginal variance. Accordingly, let  $\omega(\mathbf{x}) = \sqrt{COV(g(\mathbf{x}), g(\mathbf{x}))}$  from (4) and normalize the basis functions as  $\phi_j(\mathbf{x}) = \phi_j^*(\mathbf{x})/\omega(\mathbf{x})$ . Because this normalization is tied to the choice of covariance model it means that the basis is no longer independent of the GMRF and this linkage adds more computational overhead. However, computing  $\omega(\mathbf{x})$  can take advantage of the sparse precision matrix and we believe reducing edge effects and other artifacts is worth the extra computation.

## 3 Computational strategy and timing results

The estimators defined in the previous section can be found efficiently by a judicious use of sparse matrix decompositions and matrix identities. Most of these computations depend on the constructions of  $\Phi$ ,  $\mathbf{W}$  and  $\mathbf{Q}$  to be sparse matrices. Our basic approach exploits the fact that a sparse and positive definite matrix can be factored into a sparse cholesky decomposition. With this decomposition it is efficient to evaluate inverses and determinants. In this section we outline the key numerical steps and the reader should refer to Nychka et al. (2013) and the commented `LatticeKrig` package source code for details.

### 3.1 Spatial prediction and evaluating the likelihood

A basic calculation that illustrates the computational strategy is to evaluate  $\mathbf{M}_\lambda^{-1}\mathbf{w}$  for an arbitrary vector  $\mathbf{w}$ . Recall that  $\mathbf{M}_\lambda = \Phi\mathbf{P}\Phi^T + \lambda\mathbf{W}^{-1}$  and taken at face value  $\mathbf{M}_\lambda$  is a dense, potentially large matrix and so difficult to work with directly. The strategy is to transform  $\mathbf{M}_\lambda$  using matrix identities to involve the sparse precision matrix. The

Sherman-Morrison-Woodbury formula (Henderson and Searle (1981)) can be applied to give

$$M_{\lambda}^{-1} = (\Phi P \Phi^T + \lambda W^{-1})^{-1} = (W - (W \Phi) G^{-1} (\Phi^T W))$$

where  $G = \Phi^T W \Phi + \lambda Q$ . Because  $\Phi$ ,  $W$  and  $Q$  are all sparse,  $G$  will also be sparse and positive definite. Using this identity one can now use the sparse Cholesky decomposition for  $G$  to solve the linear system  $Gv = (\Phi^T W)w$  for  $v$  and it follows that

$$M_{\lambda}^{-1}w = Ww - W\Phi v$$

Note that an important limitation of this computational strategy is that  $\lambda$  can not be identically zero. To compute  $\hat{c}$  we use the identity  $\hat{c} = G^{-1} \Phi^T W (y - Z\hat{d})$  and exploit the sparsity of  $\Phi$  and  $W$  for multiplication and the sparse Cholesky factorization of  $G$ . Finally note that the evaluation of  $\hat{g}(x)$  can also be computed in an efficient manner if the sum is restricted to basis functions that are nonzero at  $x$ .

The other intensive computation occurs in the likelihood as the determinant of  $M_{\lambda}$ . Here we use a special case of Sylvester's Theorem: For an  $n \times m$  matrix  $U$  and identity matrices  $I_n$  and  $I_m$ ,  $|UU^T + I_n| = |U^T U + I_m|$ . Using elementary properties of matrices one can derive the identity  $|M_{\lambda}| = \lambda^{n-m} |G| / (|Q| |W|)$ . The matrices,  $W$ ,  $G$  and  $Q$  are all positive definite and sparse so the determinants can be found efficiently from the product of the diagonal elements of the Cholesky decompositions.

Based on exploiting matrix sparsity and these classic matrix identities one can evaluate the likelihood in an efficient manner. With this option we just use standard maximum likelihood methods of inference on the covariance parameters.

In this work we suggest finding the prediction errors using the well known Monte Carlo technique of conditional simulation. Under the assumption that the covariance model is known, one generates a sample from the conditional distribution of  $g$  and  $d$  given the observations. The prediction variance can be approximated from Monte Carlo draws from this conditional distribution. This computation can be done in two steps: simulating an unconditional random process at the prediction and observation locations and then determining the prediction errors based on synthetic/simulated observations for this realization. The first step is an standard application of multivariate simulation

319 by solving a linear system based on the Cholesky decomposition of the precision matrix  
320 and the second step is the same spatial estimator that is applied to actual data.

321 Here we present some timing results for the computations with the main compar-  
322 ison being with the dense matrix computations associated with Kriging. The spatial  
323 locations were uniformly distributed over the domain  $[0, 1] \times [0, 1]$  and the number  
324 were varied between 500 and 20000. The likelihood function and spatial predictions  
325 were found for an exponential covariance model and several choices of the lattice MR  
326 model. For these algorithms the computation time is dominated by basic linear alge-  
327 bra and does not depend on the values of the spatial data, the distribution of spatial  
328 locations, and the specific values of the covariance parameters. The timing is done  
329 for the function `mKrig` in the R package `fields` (Furrer et al. 2012) implementing  
330 standard Kriging and for the function `LKrig` in the R package `LatticeKrig` (Nychka  
331 et al. 2012) implementing the MR basis function model. Times reported are on a *single*  
332 processor for a Macbook Pro laptop ( 2.3 Ghz Intel Core i7, 8Gb memory) and R 3.0.1  
333 (R Development Core Team 2011). Both of these functions compute the predictions at  
334 the observations for a fixed covariance model, evaluate the likelihood and compute the  
335 coefficients for predicting the surface at arbitrary points. Despite this varied output  
336 from the functions, the Cholesky decomposition in both `mKrig` and `LKrig` dominate  
337 the time for large  $n$ .

338 Figure 1 reports the total time (“wall clock” time) for these functions using the R  
339 utility `system.time`. The dashed line is the time for the standard “Kriging” estimate  
340 using `mKrig` up to 10,000 observations and with times extrapolated to 20,000. Thus  
341 the time for 20,000 observations and standard Kriging is estimated to be about 1,300  
342 seconds (about 21 minutes). The solid black line is the time for the function `LKrig` with  
343 a single level with the number of basis functions chosen to be approximately equal to  
344 the sample size, and with the basis functions normalized to have unit marginal variance.  
345 The dotted black line is the same scheme but without normalizing the basis functions.  
346 Note that for 20000 spatial locations the times for this case are 66 seconds (normalized)  
347 and 5.4 seconds (unnormalized). The grey lines report timing with the number of basis  
348 functions keep fixed and with (solid) and without (dashed) normalization. The lines

349 labeled 10 have four levels ( $L = 4$ ) of MR and where the coarsest basis has centers  
 350 on a  $10 \times 10$  grid ( $m_x = m_y = 10$ ) and giving 7159 basis functions with nodes within  
 351 the spatial domain and 10339 total. The lines labeled 20 have coarsest grid being a  
 352  $20 \times 20$  grid ( $m_x = m_y = 20$ ) with a total of 31,259 basis functions within the spatial  
 353 domain and 37,439 total. The memory for this case is dominated by storage of the  
 354 sparse matrix  $\mathbf{G}$  comprising  $7.4 \times 10^6$  nonzero elements taking 60Mb of memory.

355 These results indicate substantial time savings over the dense matrix computations  
 356 and evaluations of the likelihood are feasible even for 20000 spatial locations. The  
 357 unnormalized computation times are particularly striking and are largely dominated  
 358 by the sparse Cholesky decomposition of the matrix  $\mathbf{G}$  discussed in Section 3. For  
 359 this work we have not exploited more efficient algorithms in the normalization step  
 360 and there is a significant difference between the normalized and unnormalized cases.  
 361 As might be expected the two covariance models with fixed number of basis functions  
 362 (“10” and “20” cases ) are closer to being linear as a function sample size. At the  
 363 sample size of approximately 10400 the  $10 \times 10$ ,  $L = 4$  case and the single level model  
 364  $103 \times 103$ ,  $L = 1$  case have equal numbers of basis functions. However, because of  
 365 the difference in levels the four level model has a  $\mathbf{G}$  with  $1.88 \times 10^6$  nonzero elements  
 366 compared to  $.67 \times 10^6$  for the one level model. This difference in sparsity explains the  
 367 timing differences for the unnormalized computations. The normalized computations  
 368 are apparently dominated by the normalization computation.

## 369 4 Properties of the covariance model

### 370 4.1 Comparison to a convolution process

371 As a foundation, we first consider a convolution approximation to the sum of radial  
 372 basis functions. First we define a single convolution process and then extend this to an  
 373 infinite mixture. Let  $z$  be a unit variance, isotropic, two dimensional Matérn process  
 374 with spatial scale parameter  $\kappa$ , smoothness  $\nu$ , and  $C_\nu(\|\mathbf{x} - \mathbf{x}'\|/\kappa) = E(z(\mathbf{x})z(\mathbf{x}'))$ ,  
 375 the corresponding covariance function. Also let  $\phi$  be a compactly supported RBF with

376  $\phi(0) = 1$ . For  $\theta > 0$  a scale parameter, define the convolution process

$$g(\mathbf{x}) = \int_{\mathbf{R}^2} \frac{1}{\theta^2} \phi(\|\mathbf{x} - \mathbf{u}\|/\theta) z(\mathbf{u}) d\mathbf{u}.$$

377 This type of process for statistical modeling is well-established (see Higdon 1998) and  
 378 as written will be Gaussian, mean zero, and have an isotropic covariance function.  
 379 Now consider a sequence of independent Matérn processes,  $z_l(\mathbf{x})$  with  $\{\theta_l\}$  a sequence  
 380 of scale parameters for the convolution kernel and “hard wire”  $\kappa_l = 1/\theta_l$ . These define  
 381 a sequence of convolution processes  $g_l(\mathbf{x})$  according to (12) with the same marginal  
 382 variance. Finally, let  $k_l$  denote the covariance function for the  $l^{\text{th}}$  process. Given,  
 383 non-negative weights  $\{\alpha_k\}$  that are summable we are lead to the MR process that is  
 384 Gaussian, mean zero and covariance given by

$$k(\mathbf{x}, \mathbf{x}') = \sum_{l=1}^{\infty} \alpha_l k_l(\mathbf{x}, \mathbf{x}').$$

385 Given this representation, a theoretical question is how the choice of  $\{\theta_l\}$  and  $\{\alpha_l\}$   
 386 influence the properties of  $k$ . In particular, is it possible to construct covariances that  
 387 represent different degrees of smoothness than those implied by the basis functions  
 388 and Matérn process used in the convolution? Typically the smoothness of an isotropic,  
 389 stationary Gaussian process is tied to the differentiability of the covariance function at  
 390 the origin. An alternative measure is to characterize the tail behavior of the spectral  
 391 density of the process. Under isotropy the spectral density will be radially symmetric  
 392 and we focus on the decay rate as  $r$  increases. In particular, for spectral densities whose  
 393 tails are bounded by a fixed polynomial decay we will take the polynomial order as a  
 394 convenient measure of the process smoothness. For the Matérn family a smoothness of  
 395  $\nu$  and dimension 2 the spectral density will have a tail behavior following  $r^{-(2\nu+2)}$  as  
 396  $r \rightarrow \infty$ . For example the exponential covariance ( $\nu = 1/2$ ) will have a spectral density  
 397 that decreases at the polynomial rate  $r^{-3}$ . A covariance spectrum with tail behavior of  
 398 the same order might be expected to provide a process model with similar smoothness  
 399 to the exponential at small spatial scales. The following theorem reports the tail  
 400 behavior for the MR process for different choices of the scale and weight sequences.  
 401 An interesting result is that the MR process can reproduce a scale of different decay

402 rates for the tail of the spectral density and can recover the -3 rate of decay for the  
 403 exponential covariance.

404 **Theorem 4.1** Assume (1)  $\phi$  is a two-dimensional Wendland covariance function of  
 405 order  $K$ . (2) the smoothness of the Matérn processes is fixed at  $\nu = 1$ . (3)  $\alpha_l = e^{-2\beta_1 l}$   
 406 and  $\theta_l = e^{-\beta_2 l}$  with  $\beta_1, \beta_2 > 0$  and  $(\beta_1/\beta_2 + 1) < (5 + 2K)$ . If  $S(r)$  denotes the spectral  
 407 density of  $g$  (or  $k$ ) with respect to the radial coordinate then there are constants  
 408 independent of  $r$ ,  $0 < A_1, A_2 < \infty$  such that

$$A_1 < S(r)r^{2\mu+2} < A_2, \text{ with } \mu = \beta_1/\beta_2.$$

409 **Corollary 4.1** Under assumptions (1) and (2) and  $\theta_l = 2^{-l}$ ,  $\alpha_l = \theta_l^{2\nu}$  and  $(\nu + 1) <$   
 410  $(5 + 2K)$ ,  $S(r)$  will have tail behavior with the same polynomial order as a two-  
 411 dimensional, Matérn process spectrum with smoothness  $\nu$ .

412 The proof of this theorem is given in the Appendix.

## 413 4.2 Numerical approximation

414 The theoretical approximation is based on a continuous convolution of the basis func-  
 415 tions with the Matérn covariance. We have found that the theoretical sequence of  
 416 weights gives an accurate approximation when 6 or more levels are considered. How-  
 417 ever this theoretical comparison does not exactly match the discrete stochastic model  
 418 used for data analysis. A more practical comparison is how well the discrete MR basis  
 419 proposed here can match members of the Matérn family. We investigate the quality  
 420 of the approximation given  $\theta_l = 2^{-l}$  but optimizing over  $\{\kappa_l\}$  and  $\{\alpha_l\}$ . Note  
 421 that this scheme is slightly different than the theoretical setup because  $\kappa_l$  is allowed  
 422 to vary independently from  $\theta_l$  and  $\alpha_l$  is not constrained to be a power of  $\theta_l$ . The most  
 423 important constraint in choosing an approximation is the initial choice of grid size ( $m_x$   
 424 and  $m_y$ ) and the number of levels,  $L$ . The spacing of the nodes should be chosen so  
 425 the coarsest level is comparable to the process correlation range and  $L$  such that the  
 426 finest basis functions have smaller scale than the finest spatial scale of the process. One  
 427 advantage of this model is that flexibility in choosing the range parameter  $\kappa$  means  
 428 that the grid spacings need not exactly conform to the correlation scale of the process.



429 The first column in Figure 2 shows the approximation for an exponential covariance  
 430 with range parameters .1, .5 and 1.0 using 3 and 4 levels of MR basis functions. The MR  
 431 parameters  $\kappa_l$  and  $\alpha_l$  have been found by minimizing the mean squared error between  
 432 the approximation and the target covariance function on a grid of 200 distances in  
 433 the interval  $[0, 1]$ . The coarsest basis function centers are organized on a  $10 \times 10$   
 434 grid on the square  $[-1, 1] \times [-1, 1]$  and so with four levels the approximation has  
 435  $10^2 + 19^2 + 37^2 + 73^2 = 7159$  two-dimensional basis functions with nodes that are  
 436 included in the spatial domain. There are 10339 basis functions total considering the  
 437 buffer regions. The plots in the upper row are the target and approximate covariances  
 438 as a function of distance from the point  $(0, 0)$  along the x-axis. The approximation  
 439 is close to being stationary and isotropic and so this comparison is representative for  
 440 distances along other orientations. In the plots the solid curve is the covariance, the  
 441 dotted line is the approximation with 3 levels, and the dashed line is the approximation  
 442 at 4 levels.

443 Not surprisingly the approximation breaks down at small distances that are below  
 444 the resolution of the finest basis functions This feature is highlighted by the plots in  
 445 the lower row where the approximation is given for points in a range close to zero.  
 446 The characters “3” and “4” indicate the smallest scale of the basis functions and  
 447 thus indicate the limits of the MR for the 3 and 4 level choices. In general it is  
 448 straightforward to improve this approximation by increasing  $L$  beyond 4. A similar  
 449 approximation is made for the Whittle covariance ( $\mu = 1$ ) except for the largest range  
 450 parameter the coarsest basis has centers on a  $5 \times 5$  grid (giving a total of 1484 basis  
 451 functions). This case is an example where the smoothness of the covariance at zero  
 452 does require as detailed basis functions and in fact we found empirically that the  
 453 courser initial grid ( $5 \times 5$ ) gives a better approximation. Note that in the error plot  
 454 there is also a small artifact, a rippling feature that is from the discrete spacing of  
 455 the basis functions. The third column of Figure 2 is an example of the ability of  
 456 the MR to approximate more general correlation functions. This is perhaps the most  
 457 strikingly example of the flexibility of this model. Here the target is a mixture of  
 458 exponentials:  $.4 \exp(-d/.1) + .6 \exp(-d/3)$ . For reference the individual exponent

459 correlation functions are plotted as grey solid lines. The approximation is also accurate  
460 with the error localized near the origin and being large below the smallest scale of the  
461 MR.

## 462 5 North American summer precipitation

463 The MR lattice model was applied to a substantive climate data set in order to test  
464 its practical value and compare it to standard Kriging. The goal is to estimate the  
465 average summer rainfall on a fine grid for North America based on high quality surface  
466 observations (NOAA/NCDC 2011). These types of fields are an important reference  
467 in studying the Earth’s climate system. GHCN data is quality controlled, curated and  
468 served by the US National Climatic Data Center and for this example we use 1720  
469 stations from North America. For each station, a least squares trend line was fit to  
470 the summer precipitation totals (June, July, August) for the period 1950-2010 and  
471 the trend line was evaluated at the midpoint time (1980.5). Note that with complete  
472 observations this is just the sample mean and we will refer to these statistics as the  
473 station “mean summer precipitation”. However, 75% of the adjusted stations are  
474 missing at least 10 values in this period and the least squares analysis will differ from  
475 a sample average.

476 The version of the climate data used is the R data set `NorthAmericanRainfall`  
477 in the `LatticeKrig` package and a spatial model was fit using stereographic map  
478 coordinates for the station locations. This projection gave spatial coordinates whose  
479 euclidean distances were similar to great circle distance (see Figure 3). The spatial  
480 model was fit to the log of mean precipitation with the spatial coordinates and elevation  
481 included as a linear fixed effects. Three correlation models were considered and we  
482 report the MLEs for the relevant parameters and the effective degrees of freedom (  
483 EDF).

484 **Matern** (2 parameters) A stationary, isotropic Matern with range and smoothness  
485 parameters.

$$486 \hat{\sigma} = .1084, \text{EDF} = 943.$$

487 **Matern-like** (2 parameters) A three-level, MR covariance with coarsest level having  
 488 a lattice of  $16 \times 13$  included the rectangular spatial domain amounting to ap-  
 489 proximately 4000 basis functions. A common value for  $\kappa$  was used to control the  
 490 range at all levels. The first MR model constrains  $\{\alpha_1, \dots, \alpha_3\}$ ,  $\alpha_k \sim 2^{-2\nu}$  with  
 491 the additional constraint that  $\sum \alpha_k = 1$ .  
 492  $\hat{\sigma} = .1402$ ,  $\hat{\nu} = .49$ ,  $\hat{\kappa} = .96$ , EDF= 489.4.

493 **Multi-resolution** (3 parameters) The same three-level structure as the Matern-like  
 494 model with  $\kappa$  a common parameter with  $\alpha_k > 0$  and  $\sum \alpha_k = 1$ .  
 495  $\hat{\sigma} = .1353$ ,  $\hat{\alpha} = (0.91, 0.00, 0.09)$ ,  $\hat{\kappa} = .7071$ , EDF= 550.6.

496 All three covariance functions include the variance parameter,  $\rho$  being the marginal  
 497 variance of the spatial process and the parameter,  $\sigma^2$ , that is the measurement error  
 498 (or nugget) variance.

499 The initial grid size for the MR models and the number of levels was identified by  
 500 trying several sizes and comparing likelihood values when models were nested. We  
 501 also avoided configurations where  $\kappa$  was large suggesting an uncorrelated model for  
 502 the GMRF. The covariance parameters were estimated by maximum likelihood and  
 503 confidence regions for the parameters were derived using the large sample chi-squared  
 504 approximation to -2 times the log likelihood. Based on a 95% confidence set the  
 505 range parameter for the Matern model was not constrained from above and so a thin-  
 506 plate spline model, i.e. a limiting process as the range becomes large, is not ruled  
 507 out. The smoothness parameter however has an MLE of .64. Figure 4 compares the  
 508 correlation functions for these three different models based on the confidence sets for  
 509 the parameters. Here the usual 95% confidence set for the model parameters based on  
 510 the likelihood was translated into a confidence band for the corresponding correlation  
 511 functions. The MR models have the flexibility to have long range correlations and  
 512 it is interesting for these data that their shape is different than the Matern family.  
 513 Also it is striking that the three level MR has  $\alpha_2 \approx 0$  suggesting omitting the middle  
 514 resolution level. The spatial predictions given by all three models are similar, however,  
 515 and within the prediction uncertainty measures. The measurement error variance is  
 516 smaller for the Matern compared to the lattice models and this is consistent with the

517 Matern representing a slightly rougher process than the MR models. In this case the  
518 Matern process captures more of the fine scale variability and so less is represented by  
519 the measurement error/nugget term.

520 Figure 5 is an example of the expected precipitation surface for a subregion over  
521 the Rocky Mountains centered on Colorado. The MR covariance with the MLE pa-  
522 rameters reported above is used for these estimates, which are evaluated on  $200 \times 200$   
523 grid. 200 conditional fields were simulated and to increase the accuracy of this sample  
524 the realizations were centered so that their mean matched their conditional expected  
525 mean, which can be computed exactly. Although the spatial model was estimated on  
526 a log scale of precipitation, the conditional samples were transformed to the raw scale  
527 of precipitation totals to represent the distribution for unlogged values. Specifically  
528 the surface in (a) is mean of the exponentiated conditional fields. Here the elevation  
529 covariate explains a large amount of the spatial structure but this component is mod-  
530 ified by the smooth nonparametric component based on the location. Plot (b) is the  
531 estimated prediction standard error as a percentage of the mean predicted field.

## 532 6 Discussions and Conclusions

533 This work has developed a new model for a spatial process: a lattice/basis model that  
534 builds on ideas from fixed rank Kriging and the computational efficiencies that are  
535 inherited from Markov random fields. The key contribution is that an independent  
536 sum of the processes at different scales can approximate a larger family of processes  
537 not limited to the properties of the covariance at each resolution level. One advantage  
538 of our model is numerical evidence that it can accurately reproduce the Matérn family  
539 of covariances. Also we give some asymptotic results based on a theoretical convolution  
540 model that indicate that a range of smoothness properties can be achieved. This result  
541 is unexpected given that the lattice/basis process has a fixed smoothness controlled by  
542 the choice of basis functions.

543 Besides the value of the lattice/basis formulation as a new covariance model there  
544 is an equally important contribution in computational efficiency for large data sets. In  
545 fact it is our perspective that more complex covariance models can only be exploited

546 when large number of observation locations allow for accurate estimation of covariance  
547 parameters. Thus efficient computation is intrinsic to entertaining new spatial models.  
548 We have been successful in identifying algorithms that allow for computing the like-  
549 lihood to estimate covariance parameters and the prediction of the spatial field using  
550 large data sets.

551 Because of the description of the stochastic spatial elements in terms of a SAR, it is  
552 straightforward to propose a non stationary extension to the lattice basis model. One  
553 would allow both the  $\kappa_l$  and  $\alpha_l$  to vary over the lattice at each level. An additional  
554 refinement would allow the SAR weights between the neighboring lattice points to  
555 be directionally dependent. In particular extending the SAR weights to the 8 first  
556 and second order neighbors can allow for a model that has directional or anisotropic  
557 dependence. The spatial variation in these parameters could be modeled by a set  
558 of covariates and fixed effects or one could include a spatial process prior on these  
559 parameter fields. The advantage of our approach and also of the related SPDE and  
560 process convolution models is that one will always obtain a valid covariance function  
561 because the model focuses on a process level description.

562 We conjecture that the choice of the Wendland family of RBFs is not crucial and  
563 other compacted supported, positive definite functions will work. Moreover by mod-  
564 ifying the distance metric to one of chordal distance one can also extend these ideas  
565 to the sphere. The one hurdle in an extension to a spherical process, however, is to  
566 devise non-rectangular grids for the nodes and to formulate a SAR on these points.

567 Finally, we note that the lattice/basis model can be implemented using a collection  
568 of simple numerical algorithms and readily available software. An R implementation  
569 is available with documented and commented source code and uses the general sparse  
570 matrix R package `spam`. The `LatticeKrig` source code is largely written in the R  
571 language with limited use of lower level C or FORTRAN functions and hence is easy  
572 to modify.

## References

- Banerjee, Sudipto, Alan E Gelfand, and Bradley P Carlin (2003), *Hierarchical modeling and analysis for spatial data*. Crc Press.
- Caragea, P. C. and R. L. Smith (2007), “Asymptotic properties of computationally efficient alternative estimators for a class of multivariate normal models.” *Journal of Multivariate Analysis*, 98, 1417–1440.
- Cressie, Noel and Christopher K Wikle (2011), *Statistics for spatio-temporal data*. Wiley. com.
- Cressie, Noel A. C. and Gardar Johannesson (2008), “Fixed rank kriging for very large spatial data sets.” *Journal of the Royal Statistical Society: Series B (Statistical Methodology)*, 70, 209–226.
- Eidsvik, Jo, Andrew O Finley, Sudipto Banerjee, and Havard Rue (2010), “Approximate bayesian inference for large spatial datasets using predictive process models.” *Computational Statistics & Data Analysis*, 56, 1362–1380.
- Fuentes, Montserrat (2007), “Approximate likelihood for large irregularly spaced spatial data.” *Journal of the American Statistical Association*, 102, 321.
- Furrer, Reinhard, Douglas Nychka, and Stephen Sain (2012), *fields: Tools for spatial data*. URL <http://www.image.ucar.edu/Software/Fields>. R package version 6.6.4.
- Henderson, H.V. and S. R. Searle (1981), “On deriving the inverse of a sum of matrices.” *SIAM Review*, 23, 53–60.
- Higdon, David M. (1998), “A process-convolution approach to modelling temperatures in the north atlantic ocean.” *Environmental and Ecological Statistics*, 5, 173–190.
- Katzfuss, Matthias and Noel Cressie (2011), “Spatio-temporal smoothing and em estimation for massive remote-sensing data sets.” *Journal of Time Series Analysis*, 32, 430–446.

599 Lindgren, Finn and Håvard Rue (2007), “Explicit construction of gmrf approximations  
600 to generalized matern fields on irregular grids.” Technical report, Lund Institute of  
601 Technology.

602 Lindgren, Finn, Håvard Rue, and Johan Lindström (2011), “An explicit link between  
603 gaussian fields and gaussian markov random fields: the stochastic partial differential  
604 equation approach.” *Journal of the Royal Statistical Society: Series B (Statistical  
605 Methodology)*, 73, 423–498.

606 Michael L. Stein, Leah J. Welty, Zhiyi Chi (2004), “Approximating likelihoods for  
607 large spatial data sets.” *Journal of the Royal Statistical Society: Series B (Statistical  
608 Methodology)*, 66, 275296.

609 NOAA/NCDC (2011). URL <http://www.ncdc.noaa.gov/ghcnm>.

610 Nychka, Douglas, Soutir Bandyopadhyay, Dorit Hammerling, Finn  
611 Lindgren, and Stephan Sain (2013), *A Multi-resolution Gaussian  
612 process model for the analysis of large spatial data sets*. URL  
613 <http://www.ucar.edu/library/collections/technotes>. NCAR Tech Note.

614 Nychka, Douglas, Dorit Hammerling, Stephen Sain, and Tia Lerud (2012),  
615 *LatticeKrig: Multiresolution Kriging based on Markov random fields*. URL  
616 <http://www.image.ucar.edu/Software/MRKriging>. R package version 2.3.

617 R Development Core Team (2011), *R: A Language and Environment for Statistical  
618 Computing*. R Foundation for Statistical Computing, Vienna, Austria, URL  
619 <http://www.R-project.org/>. ISBN 3-900051-07-0.

620 Rue, Håvard and Leonhard Held (2005), *Gaussian Markov random fields : theory and  
621 applications*, volume 104. Chapman & Hall/CRC, Boca Raton.

622 Sang, H. and J.Z. Huang (2011), “A full scale approximation of covariance functions for  
623 large spatial data sets.” *Journal of the Royal Statistical Society: Series B (Statistical  
624 Methodology)*.

625 Stein, Michael L. (2008), “A modeling approach for large spatial datasets.” *Journal of*  
626 *the Korean Statistical Society*, 37, 3.

627 Wendland, H. (1998), “Error estimates for interpolation by compactly supported radial  
628 basis functions of minimal degree.” *Journal of Approximation Theory*, 93, 258–272.

629 Wendland, Holger (1995), “Piecewise polynomial, positive definite and compactly sup-  
630 ported radial functions of minimal degree.” *AICM*, 4, 389–396.

## 631 **Acknowledgements**

632 This work supported in part by National Science Foundation grant DMS-0707069 and  
633 the National Center for Atmospheric Research. S. Bandyopadhyay is partially sup-  
634 ported by the Reidler Foundation of Lehigh University.



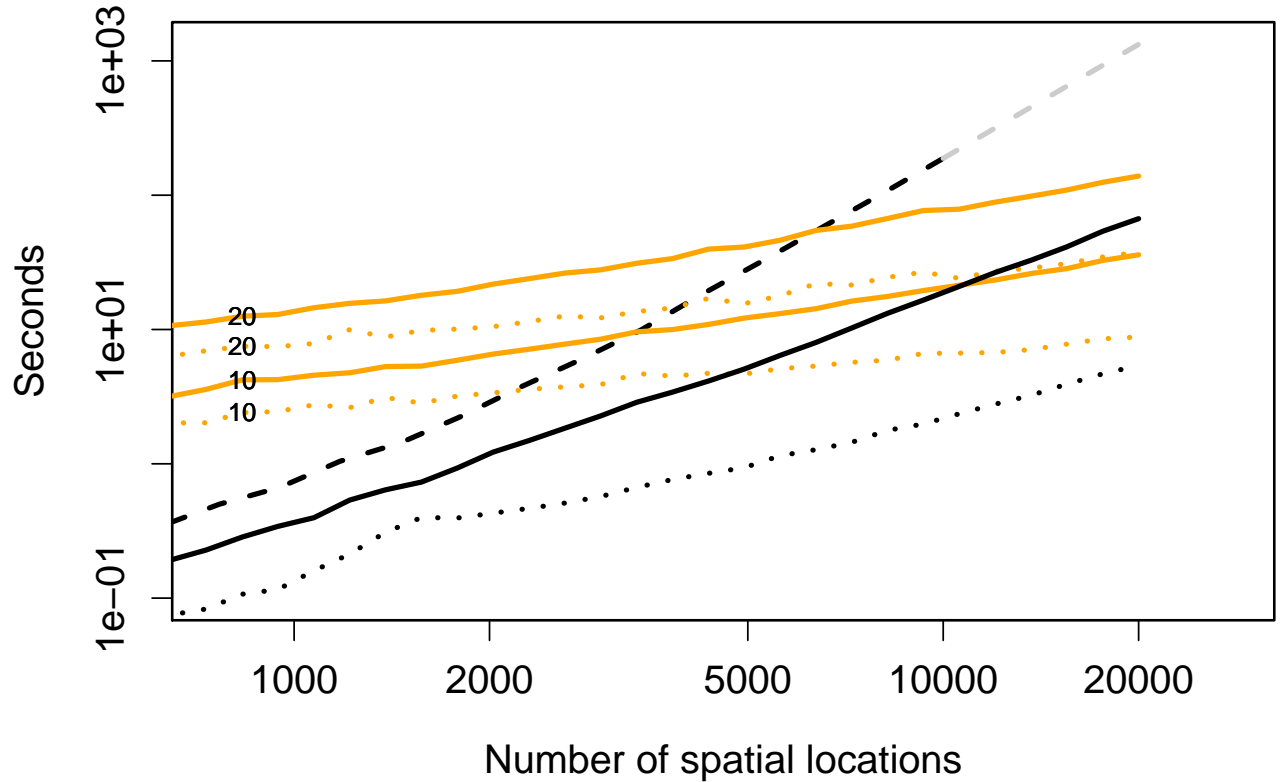


Figure 1: Timing results for the lattice/basis model and standard Kriging in seconds for several different numbers of basis functions and for the standard evaluation of the likelihood based on a dense covariance matrix. The dashed line is the time for the `mKrig` function from the `fields` R package that computes the likelihood and related statistics for an exponential covariance model with a fixed set of covariance parameters using a standard dense matrix Cholesky decomposition. Solid and dotted lines are times for the `LKrig` function from the `LatticeKrig` R package that compute the likelihood and related statistics for a MR lattice covariance with fixed parameters. Solid lines are times with normalization to a constant marginal variance and dotted lines are times without normalization. Among these cases the black lines are for a single level model where the basis functions are chosen to be roughly equal to the number of spatial locations. The orange lines use a fixed number of basis functions comprising four levels and with the coarsest level being either  $10 \times 10$  or  $20 \times 20$ . Text labels identify these cases.

Exponential covariance

Whittle covariance

Mixture:  $.4\text{Exp}(.1) + .6\text{Exp}(3.0)$

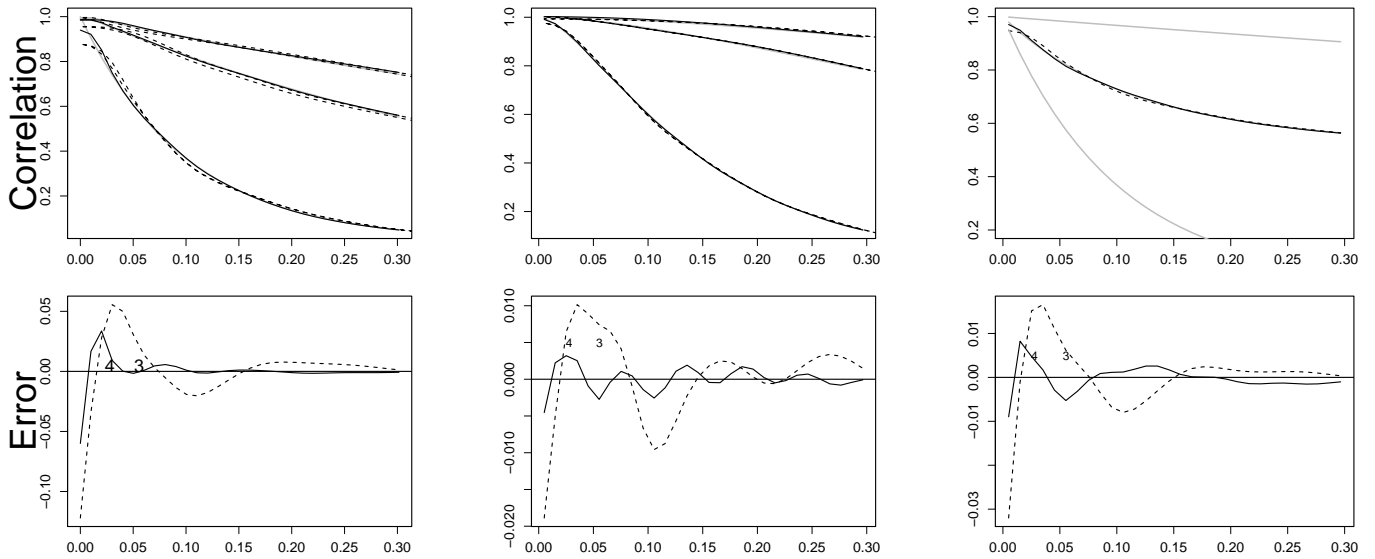


Figure 2: Approximation of Matérn covariances using the lattice/basis model. For the plots on the top row the solid grey lines are the true correlation functions. First column is an exponential correlation with range parameter  $(.1, .5 \text{ and } 1.0)$ , second column is the Whittle correlation with ranges  $.1, .5 \text{ and } 1.0$  and the third column is a mixture of two exponential correlation functions. Black lines are the approximations to these correlation functions. Approximations are indicated in black with  $L = 3$  (dashed) or  $L = 4$  (solid). The upper row is the approximations with the true correlations over the distance limits  $[0, .3]$ . The lower row are the differences between the approximation and the true correlation function for the cases when the range is  $.1$  or for the mixture model. The characters 3 and 4 indicate the support for the basis functions at the third and fourth levels of resolution.

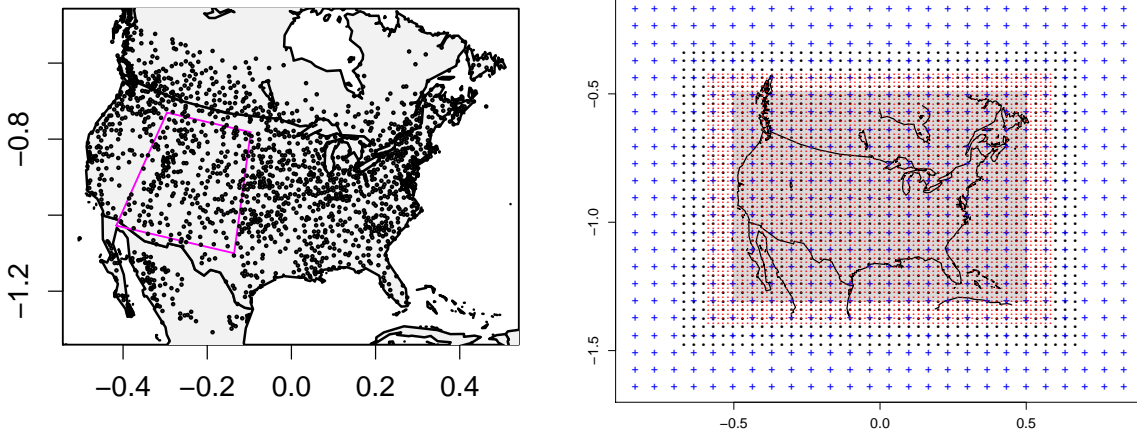


Figure 3: Illustration of the spatial domain and basis grid for the precipitation example. Left plot is a stereographic projection of precipitation location observation locations indicating the the subregion in figure 5. The right plot shows the three different grids (“+” – coarse, large dot – middle and small dot – fine) defining the nodes for the MR basis including the buffer regions of 5 extra nodes on each side to minimize edges effects. Shading indicates the rectangular spatial domain.

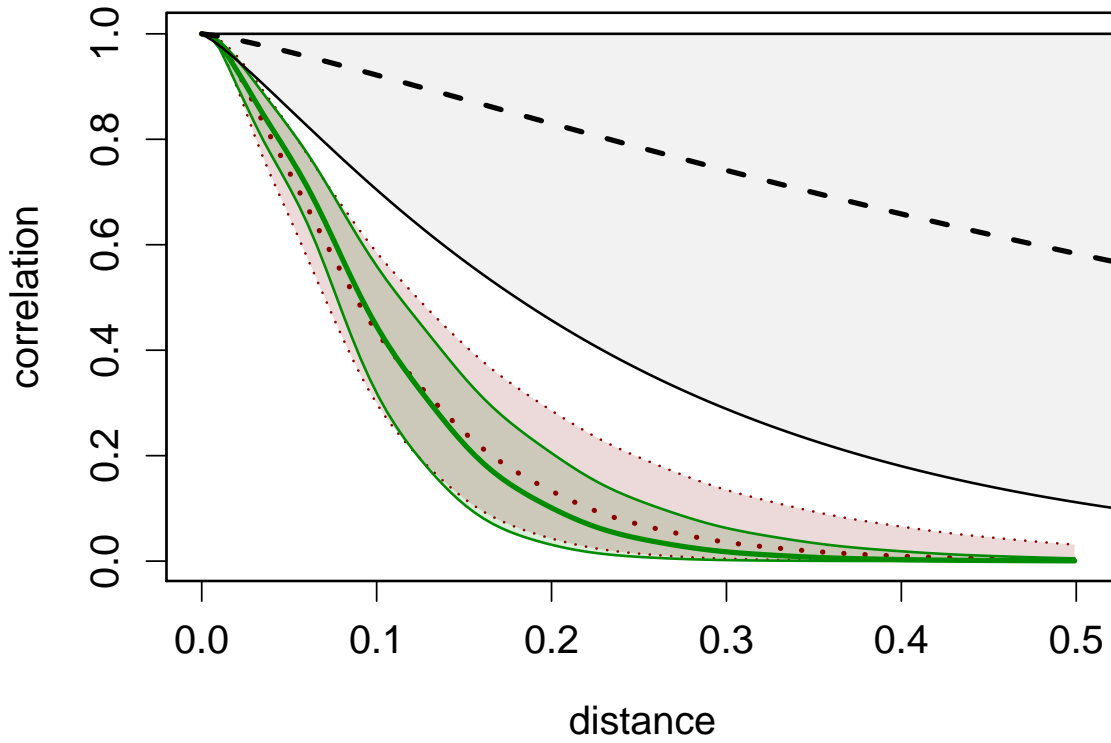


Figure 4: Correlation models fit to the precipitation data. Dashed line is the Matérn correlation function found by maximum likelihood and the light grey shading is an approximate 95% uncertainty region based on a confidence set for the range and smoothness parameters. Dotted line is the estimated correlation and uncertainty (dotted envelope) for the Matern-like covariance model. Solid line with darker shading is a similar summary for the three level MR model.

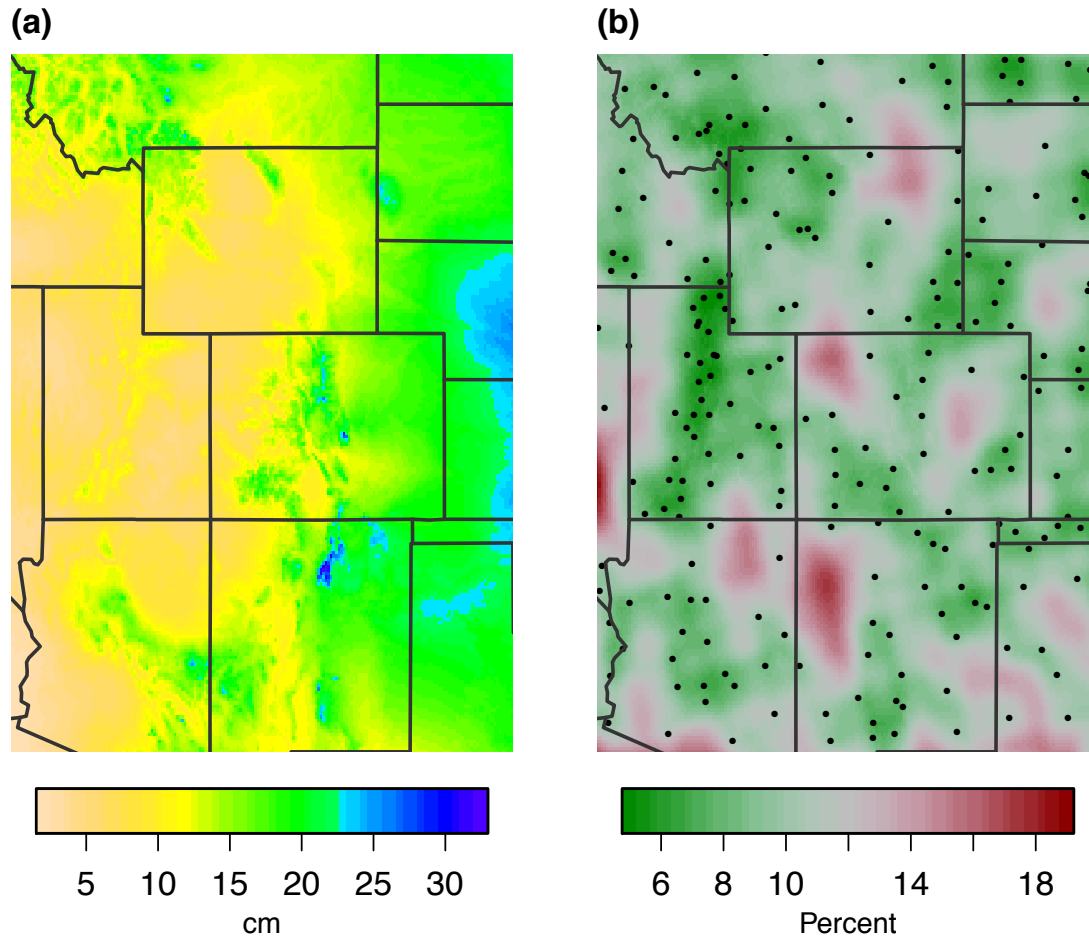


Figure 5: Plot (a) reports the spatial predictions for mean summer (June July and August) precipitation in centimeters and includes elevation as a fixed linear covariate over the Rocky Mountain region of the US. This subregion is outlined in Figure 3. The spatial covariance function is the three level MR model described in Figure 4. Plot (b) reports approximate prediction standard errors for this surface as a percentage of the predicted mean field. Solid points show observation stations.

## Appendix

Note that the convolution process has a covariance function given by

$$\int_{\mathbf{R}^2} \int_{\mathbf{R}^2} \frac{1}{\theta^4} \phi(\|\mathbf{x} - \mathbf{u}\|/\theta) C_\nu(\|\mathbf{u} - \mathbf{v}\|/\kappa) \phi(\|\mathbf{x}' - \mathbf{v}\|/\theta) d\mathbf{u} d\mathbf{v}. \quad (12)$$

### Outline of proof

Let  $\tilde{\phi}_k$  be the spectral density for  $\phi$  and  $\tilde{C}_\nu$  the spectral density of a Matérn field with  $\nu = 1$ , unit variance and unit spatial scale parameter. Including the scale parameter for the radial basis function kernel and using elementary properties of convolution.

$$\tilde{S}(r) = \sum_{l=1}^{\infty} \alpha_l \left[ \theta_l^2 \tilde{C}_\nu(\theta_l r) \right] \left[ \tilde{\phi}_k(\theta_l r) \right]^2$$

The Matérn spectral density is

$$\tilde{C}_\nu(r) = \frac{1}{(2\pi)} \frac{1}{(1+r^2)^2}.$$

For the Wendland spectral density there are constants  $C_1$  and  $C_2$  depending only on  $K$  such that for all  $\omega$

$$C_1 \leq \tilde{\phi}_k(\omega) (1 + \|\omega\|^2)^{3/2+K} \leq C_2,$$

(Wendland (1998)). Using the upper bound on  $\tilde{\phi}$ , substituting the expressions for  $\theta_l$  and  $\alpha_l$  and finally combining terms gives the upper bound

$$\tilde{S}(r) < C' \sum_{l=1}^{\infty} \alpha_l \frac{\theta_l^2}{(1 + (r\theta_l)^2)^\eta} = C' \sum_{l=1}^{\infty} \frac{e^{-2\beta_1 l} e^{-2\beta_2 l}}{(1 + (r e^{-\beta_2 l})^2)^\eta} = C' \sum_{l=1}^{\infty} \frac{e^{-(2\beta_1 + 2\beta_2)l}}{(1 + r^2 e^{-2\beta_2 l})^\eta},$$

with  $\eta = 2 + 2(3/2 + K) = 5 + 2K$ .

Now apply the useful lemma given below with the identifications  $a = 2\beta_1 + 2\beta_2$ ,  $b = 2\beta_2$  and  $c = \eta$  and  $s = r^2$ . We have the rate given by  $r^{-2(a/b)}$  and with  $2a/b = 2(2\beta_1 + 2\beta_2)/2\beta_2 = 2\beta_2/\beta_1 + 2$ . The result for the upper bound now follows and the rate for the lower bound is proved in a similar manner.

### Two Useful Lemmas

**Lemma 6.1.** *Let  $H$  be a continuous and integrable function on  $[1, \infty]$ . Also assume that  $H$  is positive and unimodal with maximum at  $u^*$ .*

$$\left| \sum_{l=1}^{\infty} H(l) - \int_1^{\infty} H(u) du \right| < H(u^*)$$

654 **Proof** Let  $L$  be the integer so that  $H(L) = \max_l H(l)$  also let  $I_l = \int_l^{l+1} H(u) du$  then  
 655 by elementary properties of the integral and the unimodality of  $H$

$$\begin{aligned} I_l &> H(l), & 1 \leq l \leq (L-1) \\ I_{l-1} &> H(l), & (L+1) \leq l \leq \infty \end{aligned} \tag{13}$$

656 summing over  $l$  gives

$$\sum_{l=1}^{\infty} I_l > \sum_{l \neq L} H(l)$$

657 Simplifying and rearranging terms

$$\int_1^{\infty} H(u) du - \sum_{l=1}^{\infty} H(l) > -H(L)$$

658 Again by properties of the integral and  $H$

$$\begin{aligned} I_{l-1} &< H(l), & 2 \leq l \leq L \\ I_l &< H(l), & (L+1) \leq l \leq \infty \end{aligned} \tag{14}$$

659 summing over  $l$  gives

$$\int_1^{\infty} H(u) du < \sum_{l \neq L} H(l)$$

660 or

$$\int_1^{\infty} H(u) du - \sum_{l=1}^{\infty} H(l) < H(L)$$

661 Noting that  $H(L) < H(u^*)$  the result now follows.

662 **Lemma 6.2.** For  $a, b, c, s > 0$  and for  $(a/b) - c < 0$  there are constants  $0 < C_1, C_2 < \infty$

$$C_1 s^{-a/b} < \sum_{l=1}^{\infty} \frac{e^{-al}}{(1 + se^{-bl})^c} < C_2 s^{-a/b}$$

663 **Proof** Based on Lemma 1 let  $H(u) = e^{-au}/(1 + se^{-bu})^c$ .  $H$  is unimodal. From basic  
 664 calculus the maximum of  $H$  is  $H(u^*) = C s^{-a/b}$  for  $0 < C < \infty$  and  $C$  depending only  
 665 on  $a, b, c$ . We now evaluate the approximating integral from Lemma 1 as a function of  
 666  $s$ .

$$\int_1^\infty H(u)du = \int_1^\infty \frac{e^{-au} du}{(1 + se^{-bu})^c} = \int_1^\infty \frac{(e^{-bu})^{a/b} du}{(1 + se^{-bu})^c}$$

667 Now make the substitution  $q = e^{-bu}$  giving  $dq = -b(e^{bu})du$  or  $du = \frac{-dq}{bq}$  and with  
 668 limits of integration,  $e^{-b}$  and 0. One obtains

$$b \int_0^{e^{-b}} \frac{q^{(a/b)-1} dq}{(1 + sq)^c} \tag{15}$$

669 Since  $(a/b) > 0$  the pole at zero is integrable and the integral is finite. Now make  
 670 the substitution  $p = sq$  giving  $dp = sdq$  and

$$b \int_0^{se^{-b}} \frac{(p/s)^{(a/b)-1} dp}{s(1 + p)^c} = bs^{-a/b} \int_0^{se^{-b}} \frac{p^{(a/b)-1} dp}{(1 + p)^c} \tag{16}$$

671 Under the assumption that  $a/b - c < 0$  the integral will be finite in the limit as  
 672  $s \rightarrow \infty$ . Thus  $\int_1^\infty H(u)du$  and  $H(u^*)$  converge to zero at the polynomial rate  $s^{-a/b}$   
 673 and the result follows from application of Lemma 1.